Available online at www.sciencedirect.com
ScienceDirect
European Journal of Mechanics B/Fluids 26 (2007) 354–366

Accurate model reduction of transient and forced wakes

Bernardo Galletti [a], Alessandro Bottaro [b], Charles-Henri Bruneau [c], Angelo Iollo [c,*]

[a] *DIASP – Politecnico di Torino, 10129 Torino, Italy*
[b] *DIAM – Università di Genova, 16145 Genova, Italy*
[c] *MAB – Université Bordeaux 1 et MC2 – INRIA Futurs, 33405 Talence, France*

Received 19 September 2005; accepted 29 September 2006

Available online 7 November 2006

Abstract

Some applications of a precise method to model the transient dynamics of large scale structures in the laminar flow past a bluff body are presented. The flow is described using empirical eigenfunctions obtained by "proper orthogonal decomposition" and the models are constructed projecting the Navier–Stokes equations onto such eigenfunctions. The linear terms in the expansion coefficients as well as in the control inputs are adjusted to exactly mimic some reference solutions. Applications shown are relative to the development of flow instabilities leading to vortex shedding and the dynamics of the vortex wake under external actuation.

Keywords: Model reduction; Proper orthogonal decomposition; Navier–Stokes

1. Introduction

Low-dimensional models involving a limited number of degrees of freedom can greatly simplify the analysis of fluid flows. The dynamics can be interpreted in terms of a small number of coherent structures that evolve and interact with one another. Low order models are also of practical interest since they can be used as "plant models" for control purposes.

Using the proper orthogonal decomposition technique (POD) [1] one can extract from an existing database of flow field snapshots, a set of orthogonal eigenfunctions. For a given number of these eigenfunctions, the average L^2 projection error of a flow snapshot is minimized by construction. As a consequence, when the flow energy is concentrated in large scale vortical structures, a small number of POD eigenfunctions captures a large fraction of the total kinetic energy of the flow. This may not always be the case since there exist applications where, even though there are large structures present in the flow, the energy spreads over so many scales that there is little hope to obtain a practical low dimensional representation [2]. In contrast, flows past bluff bodies seem to be well represented by O(10) empirical eigenfunctions when the Reynolds number is O(100) [3–5], and hence are good candidates for investigations of low dimensional models.

* Corresponding author. Full address: MAB – Université Bordeaux 1, 351, Cours de la Libération, 33405 Talence cedex. Tel.: +33 (0)5 40 00 21 57; fax: +33 (0)5 40 00 26 26.
E-mail address: angelo.iollo@math.u-bordeaux1.fr (A. Iollo).

0997-7546/$ – see front matter
doi:10.1016/j.euromechflu.2006.09.004

Even when the flow is amenable to a low dimensional description, it is not obvious that a reliable dynamical model can be obtained.

Low order models found in the literature give qualitatively reasonable results mainly for spatially confined, low Reynolds number flows. Even in such cases, there is often a divergence of the model predictions compared to the projection of the actual flow over the POD modes. In principle it should be sufficient to project the Navier–Stokes equations onto the POD eigenfunctions by a classical Galerkin approach. This way, however, one is faced with some typical problems of Galerkin approximations:

(i) how to account for boundary conditions (and eventually boundary controls);
(ii) how to devise a closure term that accounts for the unresolved modes;
(iii) how to provide adequate numerical stabilization.

The last two issues are related because usually dissipation of energy occurs mainly on the level of scales which are poorly resolved. Nevertheless the two problems are distinct, because even if a model obtained from the Navier–Stokes equations admits a bounded solution for all times, the numerical discretization could be unstable.

In the low order dynamical system of the turbulent boundary layer proposed in [6], a Heisenberg model accounted for the unresolved scales and a dissipation coefficient was tuned in order to obtain qualitatively correct results. However, to be able to use the model results for a case not previously investigated by direct numerical simulation (DNS), the amount of dissipation to be added should be known a priori. Along these lines it was proposed [7] to adjust the dissipation parameter so as to balance the energy budget for each POD mode. This way it was possible to reduce the error between the dynamical system predictions and the DNS projection over the POD modes. Nevertheless, an exponential divergence in time between the DNS and the model results persists.

In further studies it was recognized that a straightforward POD-Galerkin approximation of a model problem – a scalar linear advection equation – was numerically unstable [8,9]. In that case there was no question of lack of dissipation because of missing scales; it was a pure numerical effect. Moreover, it was shown that the POD-Galerkin projection for such a simple case is equivalent to a finite difference centered spatial discretization, and that the effect of truncating the Galerkin expansion was at most that of enlarging the stability bounds of the POD-Galerkin scheme. In addition, it was proved that selecting an appropriate norm in the definition of the empirical eigenfunctions as well as in the Galerkin projection, the low order models obtained displayed better stability properties, as recently confirmed in [10].

Clearly, low Reynolds number simulations suffer much less from numerical instabilities because of physical viscosity, and hence the corresponding POD models are not affected by instabilities if a sufficient number of POD modes are taken into account [3,4]. Even for such cases, though, the long term dynamics predicted by the low order model may deviate significantly from reference DNS results as shown in [11]. As a remedy a dissipative model based on spectral viscosity was proposed therein. The cut-off parameters were selected based on bifurcation analysis, i.e., by matching the attractor of the low order model to that predicted by DNS.

The idea of fitting the POD model results to those of DNS is attractive since it may solve some of the physical modeling issues as well as the problem of numerical drifts. In this sense in [12] it was proposed to calibrate the linear term in the Galerkin model resulting from projecting the Navier–Stokes equations over the POD modes, in order to achieve a best fit for a number of reference time-dependent flow solutions. In particular, it was shown that such calibration leads to a model that correctly reproduced the main flow features for Reynolds numbers other than those from which the model was derived. Similar approaches have been recently undertaken for moderately to complex flows [13–15].

The purpose of this paper is to improve the calibration procedure presented in [12] and extend it in order to model the transient dynamics of coherent structures. Two test cases are considered: the development of a flow instability leading to vortex shedding and the dynamics of a vortex wake under the effect of transverse flow due to wall-mounted actuators.

2. Model reduction

We consider the flow around a square cylinder symmetrically placed between semi-infinite parallel walls (Fig. 1). The inlet velocity profile is parabolic. For a blockage ratio L/H of 0.125, this flow is believed to be two-dimensional

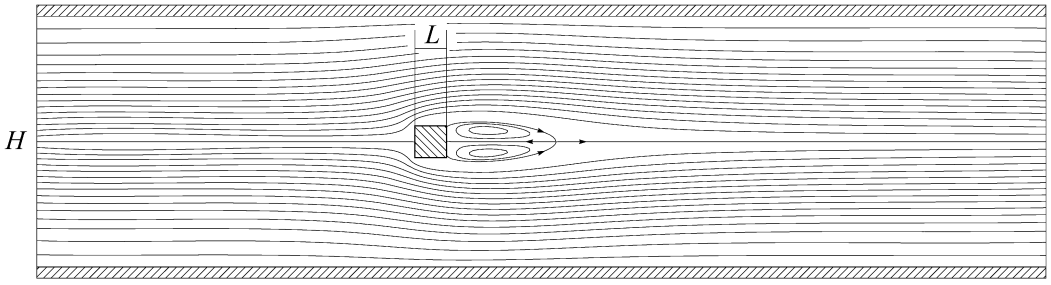

Fig. 1. Definition of the geometry and streamlines of the unstable, steady solution $\bar{\boldsymbol{u}}(\boldsymbol{x})$ at $Re = 66$.

and laminar as long as the Reynolds number based on the square side L is below 255 [16–19]. The flow field data are obtained by numerical integration of the incompressible Navier–Stokes equations. The integration scheme as well as the computational parameters, like channel length and cylinder position, are the same as in [12]. We refer the reader to that study for the computational details and for the validation of the numerical results. Unless otherwise stated, all the quantities considered are non-dimensional: the reference values for the normalization are the length L of the side of the square cylinder, the centerline velocity at the inlet section U, the dynamic pressure ρU^2 and the time scale $T_{\text{ref}} = L/U$.

The velocity field database is arranged as a set of N vectors $\{\mathbf{U}^{(1)}, \mathbf{U}^{(2)}, \ldots, \mathbf{U}^{(N)}\}$, where each vector represents a snapshot of the velocity field at a given time. Let us subtract the steady, unstable solution[1] $\bar{\mathbf{U}}$ from each snapshot and consider the new set of snapshots $\mathbf{W}^{(n)} = \mathbf{U}^{(n)} - \bar{\mathbf{U}}$, $n = 1, \ldots, N$. The aim is to find a low dimensional subspace of $\mathcal{L} = \text{span}\{\mathbf{W}^{(1)}, \mathbf{W}^{(2)}, \ldots, \mathbf{W}^{(N)}\}$ that gives the best approximation of $\mathcal{L}$. To this end we define a unit norm vector $\boldsymbol{\phi}$ that has the same structure of the snapshots and the largest mean square projection on the elements of $\mathcal{L}$. Following Sirovich's ideas [20] $\boldsymbol{\phi}$ is expressed as a linear combination of the snapshots, $\boldsymbol{\phi} = \sum_{n=1}^{N} b_n \mathbf{W}^{(n)}$, leading to the eigenproblem $\mathbf{R}\boldsymbol{b} = \lambda \boldsymbol{b}$, where $R_{ks} = \mathbf{W}^{(k)^{\mathrm{T}}} \mathbf{W}^{(s)}$ and $\mathbf{b} = [b_1, b_2, \ldots, b_N]^{\mathrm{T}}$. The solution of the eigenproblem yields N eigenvectors $\boldsymbol{\phi}_n$ (the discrete POD modes) that form a complete orthonormal set for $\mathcal{L}$. The discrete instantaneous velocity can be expanded in terms of the discrete POD eigenmodes: $\boldsymbol{u}(\boldsymbol{x}, t) = \bar{\boldsymbol{u}}(\boldsymbol{x}) + \sum_{n=1}^{N_m} a_n(t) \boldsymbol{\phi}_n(\boldsymbol{x})$. The main property of this basis is that most of the flow energy is captured using a number $N_m \ll N$ of functions $\boldsymbol{\phi}_n$.

2.1. POD-Galerkin model

An accurate model of the developing instability is obtained by a Galerkin projection of the incompressible Navier–Stokes equations over the POD modes. The resulting low order model is

$$\begin{aligned} &\dot{a}_r(t) = \left(A'_r + A''_r\right) + \left(C'_{kr} + C''_{kr}\right) a_k(t) - B_{ksr} a_k(t) a_s(t), \\ &a_r(0) = \left(\boldsymbol{u}(\boldsymbol{x}, 0) - \bar{\boldsymbol{u}}(\boldsymbol{x}), \boldsymbol{\phi}_r\right), \end{aligned} \tag{1}$$

where the Einstein summation convention is used and all the subscripts run from 1 to N_m. The coefficients A''_r, B_{ksr} and C''_{kr} derive directly from the Galerkin projection of the Navier–Stokes equations onto the POD modes and are defined by

$$\begin{aligned} B_{ksr} &= (\boldsymbol{\phi}_k \cdot \nabla \boldsymbol{\phi}_s, \boldsymbol{\phi}_r), \\ C''_{kr} &= -(\bar{u} \cdot \nabla \boldsymbol{\phi}_k, \boldsymbol{\phi}_r) - (\boldsymbol{\phi}_k \cdot \nabla \bar{u}, \boldsymbol{\phi}_r) + (\Delta \boldsymbol{\phi}_k, \boldsymbol{\phi}_r)/Re, \\ A''_r &= -(\bar{u} \cdot \nabla \bar{u}, \boldsymbol{\phi}_r) + (\Delta \bar{u}, \boldsymbol{\phi}_r)/Re, \end{aligned}$$

where $(\cdot, \cdot)$ is the canonical L^2 inner product; the terms A'_r and $C'_{kr}\, a_k(t)$ are added in order to model the interaction of the unresolved modes with the resolved ones. They also take into account the effect of the pressure drop along the channel $(\nabla p, \boldsymbol{\phi}_r)$, as argued in the following.

[1] A description of how this base flow is obtained is given in Section 3.

Let us consider the projection of the pressure term: thanks to the fact that the POD modes are divergence free by construction and that they vanish on the walls, we have

$$(\nabla p, \boldsymbol{\phi_r}) = \int_{out} p\phi_r^u \,\mathrm{d}s - \int_{in} p\phi_r^u \,\mathrm{d}s,$$

where *out* is the outlet and *in* is the inlet of the channel and ϕ_r^u is the first component of the POD mode ϕ_r. In general we subtract from the flow snapshots a reference solution that verifies the same boundary conditions as the actual flow we consider. Hence, the POD modes are 0 at the inlet and therefore the second integral on the right hand side of the expression above is 0. If the channel is long enough, diffusion will smooth the flow past the cylinder until we finally get a steady velocity profile identical to that of the steady unstable solution, meaning that the POD modes will vanish at the outlet as well. As a consequence, the first integral above is also 0. Of course, in our computations this is only approximately true. Furthermore, since we limit our Galerkin expansion to a finite number of modes, we miss the feedback of those unresolved modes onto the resolved ones. However, we could in principle write the solution of the equation for the unresolved modes as a function of the resolved ones and then inject this solution in the equation for the resolved modes. Of course we do not have such an explicit solution, but we can write its MacLaurin expansion up to the linear term. The calibration terms that we add to the equation can be interpreted as the coefficients of such expansion.

By setting $A'_r = A_r - A''_r$ and $C'_{kr} = C_{kr} - C''_{kr}$ system (1) reads

$$\begin{aligned} &\dot{a}_r(t) = f_r(a_1, \ldots, a_{N_m}, A_r, C_{kr}) = A_r + C_{kr}a_k(t) - B_{ksr}a_k(t)a_s(t), \\ &a_r(0) = \big(\boldsymbol{u}(\boldsymbol{x}, 0) - \bar{\boldsymbol{u}}(\boldsymbol{x}), \boldsymbol{\phi}_r\big). \end{aligned} \tag{2}$$

In view of the orthogonality of the POD modes, the inner product of the i-th snapshot and the r-th mode represents the reference value of coefficient $a_r(t)$ computed at the time t_i, that is $\hat{a}_r(t_i) = (\mathbf{W}^{(i)}, \boldsymbol{\phi}_r)$. Since the snapshots of the flow are N, there will be a discrete set of N reference values for each amplitude $a_r(t)$. We can pass from the discrete to the continuous setting in the time variable by defining $\hat{a}_r(t)$ as the spline interpolating the set of points $\{[t_1, \hat{a}_r(t_1)], \ldots, [t_N, \hat{a}_r(t_N)]\}$.

At this point the coefficients A_r, C_{kr} can be found so that the amplitude coefficients $a_r(t)$, computed by solving (2), are as close as possible to the corresponding reference amplitudes $\hat{a}_r(t)$. Recalling that $T = t_N$, this objective is reached by minimizing the functional

$$\int_0^T \sum_{r=1}^{N_m} \big(a_r(t) - \hat{a}_r(t)\big)^2 \,\mathrm{d}t$$

under the constraints (2). The previous problem is equivalent to finding the unconstrained extremum of the functional:

$$\mathcal{J} = \int_0^T \sum_{r=1}^{N_m} \big(a_r(t) - \hat{a}_r(t)\big)^2 \,\mathrm{d}t + \int_0^T b_k\big[\dot{a}_k(t) - A_k - C_{lk}a_l(t) + B_{lsk}a_l(t)a_s(t)\big]\,\mathrm{d}t,$$

where b_k is the appropriate Lagrange multiplier. To this end the vanishing of the Fréchet derivatives of $\mathcal{J}(a_r(t), b_r(t), A_r, C_{kr})$ with respect to all of its arguments must be imposed. This leads to the following optimality problem

$$\begin{cases} \dot{a}_r(t) = A_r + C_{kr}a_k(t) - B_{ksr}a_k(t)a_s(t), \\ a_r(0) = \big(\boldsymbol{u}(\boldsymbol{x}, 0) - \bar{\boldsymbol{u}}(\boldsymbol{x}), \boldsymbol{\phi}_r\big), \end{cases} \quad \text{direct problem,} \tag{3}$$

$$\begin{cases} -\dot{b}_r(t) = \big[C_{rk} - (B_{lrk} + B_{rlk})a_l(t)\big]b_k(t) - 2\big[a_r(t) - \hat{a}_r(t)\big], \\ b_r(T) = 0, \end{cases} \quad \text{adjoint problem,} \tag{4}$$

$$\begin{cases} \int_0^T b_r(t)\,\mathrm{d}t = 0, \\ \int_0^T a_k(t)b_r(t)\,\mathrm{d}t = 0, \end{cases} \quad \text{optimality conditions,} \tag{5}$$

where all of the subscripts go from 1 to N_m. These equations are discretized with a pseudo–spectral collocation method along the t axis. The functions $a_r(t), b_r(t)$ and $\hat{a}_r(t)$ are sampled at the N_t Gauss–Lobatto points $t_i = T/2(1 - \xi_i)$

with $\xi_i = \cos\pi(i-1)/(N_t-1)$ and $i = 1,\ldots,N_t$, that is $a_{ir} = a_r(t_i), b_{ir} = b_r(t_i)$ and $\hat{a}_{ir} = \hat{a}_r(t_i)$. An interpolation is performed to retrieve the values of the functions away from the nodal points t_i, more precisely

$$a_r(t) \approx \sum_{j=1}^{N_t} \psi_j\left(1-\frac{2}{T}t\right)a_{jr},$$

$$b_r(t) \approx \sum_{j=1}^{N_t} \psi_j\left(1-\frac{2}{T}t\right)b_{jr},$$

$$\hat{a}_r(t) \approx \sum_{j=1}^{N_t} \psi_j\left(1-\frac{2}{T}t\right)\hat{a}_{jr},$$

where $\xi = 1-2t/T$ and $\psi_j(\xi)$ are the Lagrange interpolating polynomials based on the nodes ξ_i. The time derivatives of the first two interpolated functions at the nodal values are then

$$\begin{aligned}\dot{a}_r(t_i) &\approx -\frac{2}{T}\sum_{j=1}^{N_t}\left.\frac{\mathrm{d}\psi_j}{\mathrm{d}\xi}\right|_{\xi_i} a_{jr} = \sum_{j=1}^{N_t} D_{ij}\,a_{jr},\\ \dot{b}_r(t_i) &\approx -\frac{2}{T}\sum_{j=1}^{N_t}\left.\frac{\mathrm{d}\psi_j}{\mathrm{d}\xi}\right|_{\xi_i} b_{jr} = \sum_{j=1}^{N_t} D_{ij}\,b_{jr}.\end{aligned} \tag{6}$$

The differentiation matrix can be found in [21] and is equal to

$$D_{ij} = -\frac{2}{T}\left.\frac{\mathrm{d}\psi_j}{\mathrm{d}\xi}\right|_{\xi_i} = -\frac{2}{T}\begin{cases}\dfrac{c_i}{c_j}\dfrac{(-1)^{j+i}}{\xi_i-\xi_j}, & j\neq i,\\ -\dfrac{1}{2}\dfrac{\xi_i}{1-\xi_i^2}, & j=i\neq 1,N_t,\\ \dfrac{2(N_t-1)^2+1}{6}, & j=i=1,\\ -\dfrac{2(N_t-1)^2+1}{6}, & j=i=N_t\end{cases}$$

with $c_1 = c_{N_t} = 2$ and $c_2 = \cdots = c_{N_t-1} = 1$.

The optimality condition can be rewritten in terms of the interpolated functions as follows

$$\int_0^T a_k(t)b_r(t)\,\mathrm{d}t \approx \sum_{i=1}^{N_t}\sum_{j=1}^{N_t} a_{ik}I_{ij}b_{jr}, \tag{7}$$

where the integrals

$$I_{ij} = \int_0^T \psi_i(\xi)\psi_j(\xi)\,\mathrm{d}\xi \quad \text{with } i,j = 1,\ldots,N_t$$

are calculated by means of Legendre quadrature. Finally, by virtue of (6) and (7), Eqs. (3)–(5) are discretized as follows

$$\begin{aligned}&a_{1r} = a_r(0), \qquad r = 1,\ldots,N_m,\\ &D_{ij}a_{jr} - A_r - C_{lr}a_{il} + B_{lsr}a_{il}a_{is} = 0, \quad i = 2,\ldots,N_t,\ r = 1,\ldots,N_m,\\ &D_{ij}b_{jr} + C_{rs}b_{is} - (B_{lrs}+B_{rls})a_{il}b_{is} - 2[a_{ir}-\hat{a}_{ir}] = 0, \quad i = 1,\ldots,N_t-1,\ r = 1,\ldots,N_m,\\ &b_{N_tr} = 0, \quad r = 1,\ldots,N_m,\end{aligned}$$

$$\mathbf{1}_i I_{ij} b_{jr} = 0, \quad r = 1, \ldots, N_m,$$
$$a_{ik} I_{ij} b_{jr} = 0, \quad k = 1, \ldots, N_m,\ r = 1, \ldots, N_m,$$

where $\mathbf{1}$ is a N_t-dimensional array of ones. These are $2N_t N_m + N_m + N_m^2$ algebraic equations in the $2N_t N_m + N_m + N_m^2$ unknowns and are solved with a Newton method which converges rapidly. The number N_t must be large enough to produce a good description of the high frequency behavior of the amplitude coefficients, consequently it should be increased with the increase of N_m. The reason why we choose to apply a spectral approximation, taking care to respect such approximation in integrals and derivatives, is that it allows an exponential accuracy in approximating the dynamics of the reference data.

The former procedures can be interpreted as a calibration of the model on the given database. Compared to the method used in [12], this approach is more efficient and accurate. It is more efficient because the solution is obtained by solving the direct and adjoint problem in one shot. This approach is useful because it allows the solution of problems which would normally be out of reach using a direct/adjoint iteration and a gradient method. The fact of using a spectral method to solve the calibration problem is important because of the exponential accuracy of the reference solution that can be achieved, allowing for example the analyses reported in the next sections.

3. Low dimensional modeling of the developing instability

The frequency and amplitude of the oscillations of the flow in the wake are computed at several values of the Reynolds number between 60 and 70. Extrapolating to 0 the oscillation amplitude of the lift coefficient as a function of the Reynolds number, it is found that – in the present configuration – the critical value for the onset of periodic flow is approximately $Re = 57$.

We consider a numerical database of the flow developing out of the unstable, steady solution at $Re = 66$. For such low Reynold numbers, the vortex shedding transient is very long. For this reason, after impulsive start, the flow solution settles down to an almost steady state from which it departs very slowly. We select as steady unstable solution the flow snapshots that has minimal time residual before the vortex shedding takes place. This snapshot is indeed symmetrical, see Fig. 1. From there on, the DNS indicates that the transient lasts about 95 units of time (non-dimensional time multiplied by T_{ref}), until the limit cycle solution is attained.

Our intent is to simulate the initial part of the transient originating from the steady, unstable solution at $Re = 66$. Beginning from such a solution a simulation lasting 40 units of time was performed. A model like the one of Eq. (2) can be deduced from such a database, with the unknowns A_r, C_{kr} calculated according to the procedure described above.

The 4 POD modes depicted in Fig. 2 are used for the model. The first two modes basically capture the wake oscillation, whereas the last two modes are shift modes [5] that take into account the evolution in time of the base flow from the steady unstable solution. With $N_m = 4$, we have the following error in terms of reconstructed flow energy:

$$\frac{1}{N}\sum_{i=1}^{N} \frac{\|\mathbf{W}^{(i)} - \sum_{n=1}^{N_m} (\mathbf{W}^{(i)}, \boldsymbol{\phi}_n)\boldsymbol{\phi}_n\|}{\|\mathbf{U}^{(i)}\|} = 5.0 \times 10^{-5}$$

hence the retained modes represent basically all of the energy in the flow database. Using more modes is of no benefit because the corresponding POD modes fall into numerical noise. Using less modes does not allow to take into account shift modes. In Fig. 3 (left and middle) the solution of the model in terms of the time evolution of the coefficients $a_i(t)$ is compared to the reference Navier–Stokes solution projected onto the POD modes. The model is able to exactly reproduce the dynamics of the considered part of the transient. Without properly accounting for unresolved modes, boundary conditions or numerical stabilization, the model simply diverges after a few time steps within the snapshot sampling region.

In perfect analogy with what one would do in a stability study using a full order model, we compute the growth rate of the instability using Eq. (2). The equation is linearized about the equilibrium state $a_r(0) = 0$ with $r = 1, \ldots, N_m$ which corresponds to the unstable solution of the steady Navier–Stokes equations for $Re = 66$. Expanding f_r as a power series about this equilibrium point and neglecting the second order terms one obtains: $\dot{a}_r(t) = f_r(0, A_r, C_{kr}) + J_{rj} a_j(t)$ where $J_{rj} = (\partial f_r/\partial a_j)_0 = C_{jr}$. From $\dot{a}_r(0) \simeq 0$ it follows that $A_r \simeq 0$; this fact is confirmed numerically

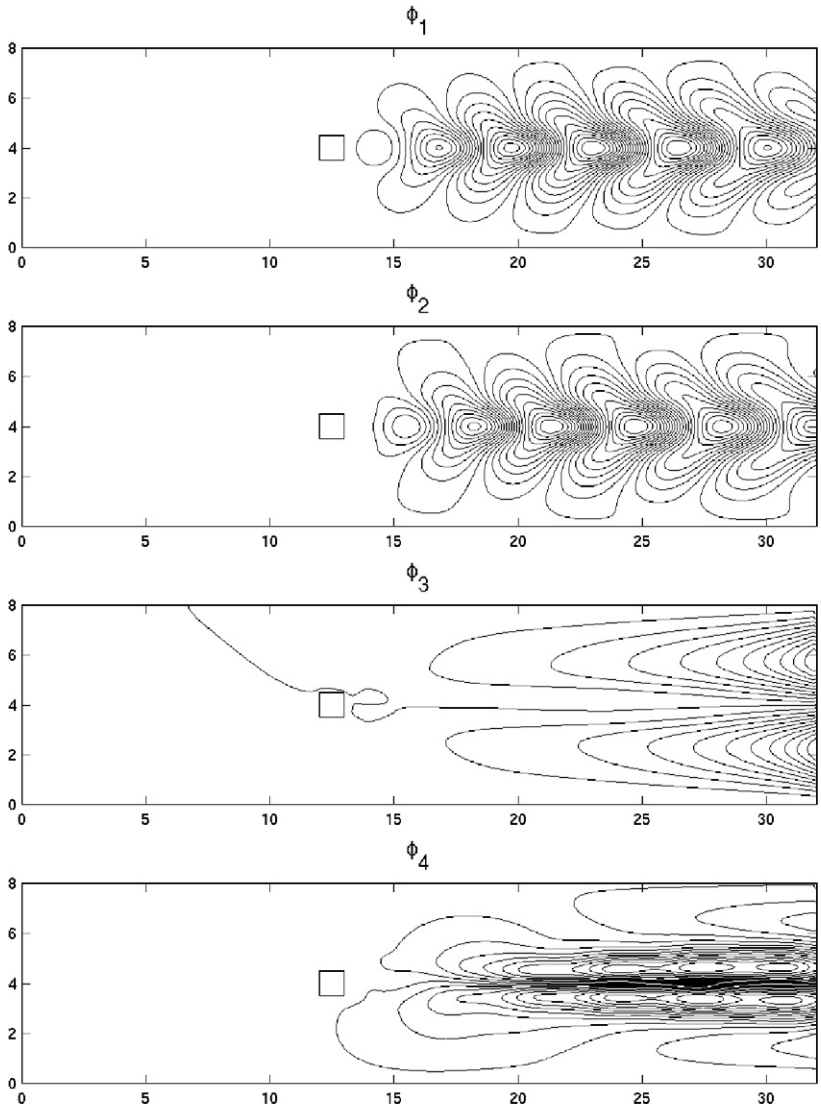

Fig. 2. Modes used for the model. The stream function (for given x, the integral of the first component of ϕ vs. y) pertinent to each mode is depicted.

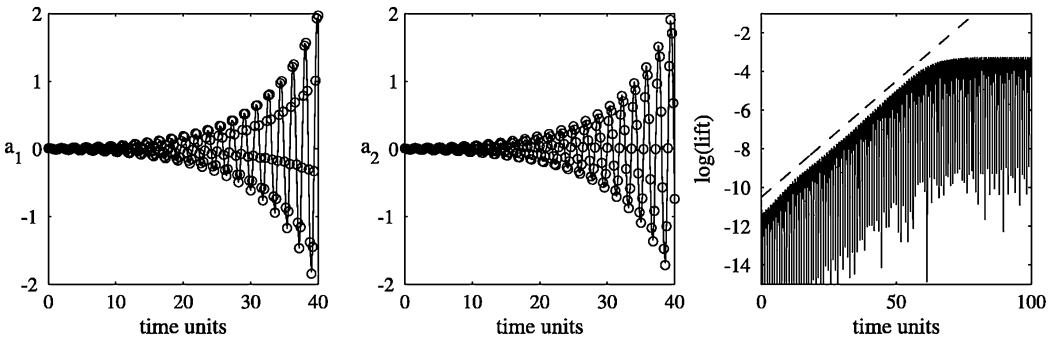

Fig. 3. Left and middle pictures: prediction of the model calibrated between 0 and 40 time units of the transient. Comparison between the mode amplitudes of model integration (solid lines) and the projection of the numerical simulation over the corresponding modes (circles). Right picture: logarithm of the absolute value of the lift in the transient regime (solid line) and a line (dashed) of slope $\mathrm{Re}(\lambda_1)/T_{\mathrm{ref}}$.

since the coefficients A_r found are of order 10^{-4}. As a result $f_r(0, A_r, C_{kr}) \simeq 0$, so that the linearized state equation reads

$$\boldsymbol{a}_t(t) = \mathbf{J}\boldsymbol{a}(t). \tag{8}$$

The solution is

$$\boldsymbol{a}(t) = \mathbf{Q}\exp(\boldsymbol{\Lambda} t)\mathbf{Q}^{-1}\boldsymbol{a}(0) \tag{9}$$

with $\boldsymbol{a}(t) = [a_1(t), \ldots, a_{N_m}(t)]^{\mathrm{T}}$, $\boldsymbol{\Lambda}$ the $N_m \times N_m$ diagonal matrix corresponding to the eigenvalues of $\mathbf{J} = \{J_{rj}\}_{1 \leqslant r,j \leqslant N_m}$ and $\mathbf{Q}$ the $N_m \times N_m$ matrix whose columns are the corresponding right eigenvectors. The numerical values rounded off to two decimal places are $\lambda_1 = 0.03 + 0.74\mathrm{i}$, $\lambda_2 = 0.03 - 0.74\mathrm{i}$, $\lambda_3 = -0.16$, $\lambda_4 = -0.09$ and

$$\mathbf{Q} = \begin{bmatrix} 0.71 & 0.71 & -0.10 & -0.02 \\ -0.00 + 0.70\mathrm{i} & -0.00 - 0.70\mathrm{i} & -0.03 & -0.10 \\ -0.00 - 0.00\mathrm{i} & -0.00 + 0.00\mathrm{i} & -0.32 & -0.92 \\ -0.00 - 0.00\mathrm{i} & -0.00 + 0.00\mathrm{i} & -0.94 & -0.37 \end{bmatrix}.$$

There are two complex conjugate eigenvalues with positive real part, λ_1 and λ_2. The eigenvectors pertinent to λ_1 and λ_2 are just the first two POD modes (with a phase shift of $\pi/4$). We conclude that the only unstable modes relative to this flow are represented by the first and second POD modes. The imaginary parts of λ_1 and λ_2 correspond to a non-dimensional frequency of $\mathrm{Im}(\lambda_1)/(2\pi) = 0.119$ whereas the non-dimensional vortex shedding frequency of the fully developed flow is 0.124. Unsurprisingly, the growth rate of the instability is very close to that predicted by the real part of λ_1, as illustrated in Fig. 3 (right). We conclude that the most energetic unsteady POD modes, extracted from a DNS of the transient state, give a reliable representation of the instability of this flow.

In order to assess the capability of the POD-Galerkin model to give good predictions for times longer than those upon which the model was built, a time integration of the model itself has been performed beyond $t = 40$ and up to a time of 100, corresponding to the fully developed flow. The amplitudes so-computed have been compared to the projections of the flow snapshots taken from the integration range onto the given POD modes. The snapshots between the time units 40 and 100 are reconstructed by the POD modes relevant to the interval 0–40 with an average error of about 5%. In Fig. 4(a) a comparison is shown between the amplitude coefficient resulting from model integration and the corresponding reference amplitude obtained by projection. The solution is accurately extrapolated for several shedding cycles, but for larger times a slight phase drift as well as an error in the oscillation amplitude prediction is remarked. A possible remedy for this problem was proposed in [22]. One can notice, however, that the model is able to predict the length of the transient, as both the computed and the projected amplitudes saturate in approximately the same time. The above procedure has been repeated by extracting a POD base from a database of 145 snapshots between the time instants 28.4 and 35.6, and by calibrating a four dimensional POD-Galerkin model over the same time interval. The results depicted in Fig. 4(b) are quite similar to the previous ones, showing that the same amount of information can be captured by taking snapshots from a narrow time interval in the first part of the transient.

3.1. Unstable mode estimation

Let us now compare the most unstable mode obtained by the above reduced model to the one obtained by the method proposed in [23], where the full order problem, i.e. the incompressible Navier–Stokes equations, linearized about the steady unstable solution $\bar{\mathbf{U}}$, is used. To this end let $\mathbf{L}$ denote the linearization of the Navier–Stokes discretization operator in space, once the incompressibility constraint is satisfied. The resulting semidiscretization valid in the vicinity of $\bar{\mathbf{U}}$ can be written as

$$\boldsymbol{\psi}_t = \mathbf{L}\boldsymbol{\psi}, \tag{10}$$

where $\boldsymbol{\psi}(t) = \mathbf{U}(t) - \bar{\mathbf{U}}$ is a column vector which contains the grid values of the velocity components arranged with the same rules as they are organized in the snapshots vectors. The dimensions of $\boldsymbol{\psi}$ and $\mathbf{L}$ are $2M \times 1$ and $2M \times 2M$ respectively, with M the number of grid points. The solution of Eq. (10) can be written as

$$\boldsymbol{\psi}(t) = \mathbf{P}\exp(\boldsymbol{\Sigma} t)\mathbf{P}^{-1}\boldsymbol{\psi}_0, \tag{11}$$

where $\boldsymbol{\psi}_0$ is the initial condition corresponding to the steady unstable solution, $\boldsymbol{\Sigma}$ is the diagonal matrix containing the eigenvalues of $\mathbf{L}$ and $\mathbf{P}$ is the matrix whose columns are the corresponding eigenvectors such that $\mathbf{LP} = \mathbf{P}\boldsymbol{\Sigma}$.

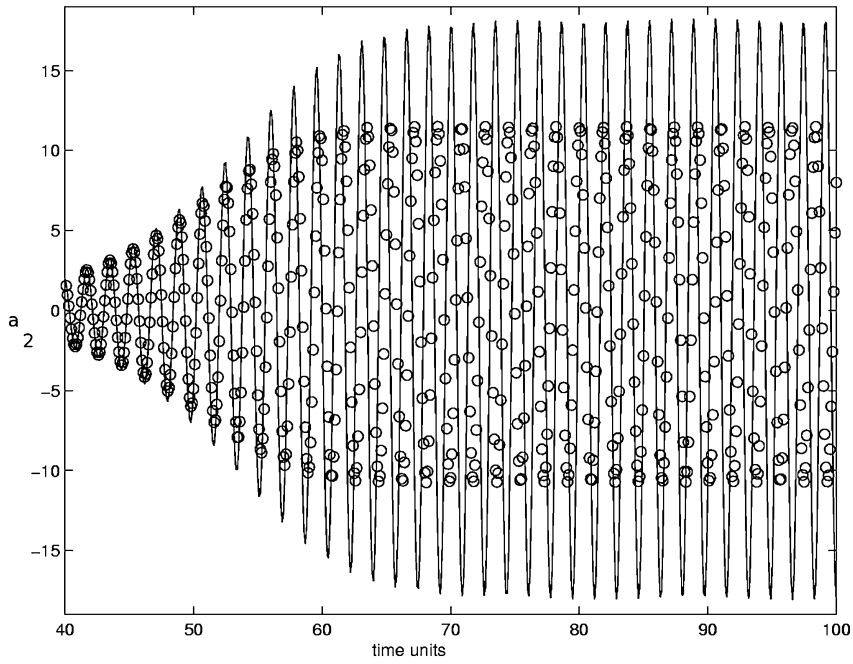

(a)

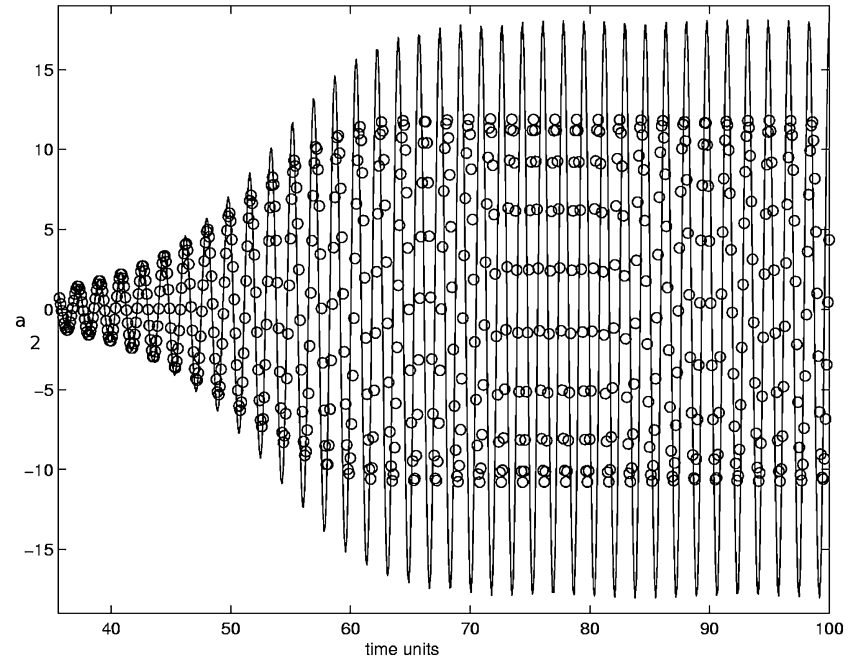

(b)

Fig. 4. (a) Prediction over the whole transient of the model calibrated on the time range 0–40: comparison between the second mode amplitude from model integration $a_2(t)$ (thick line) and numerical simulation $\hat{a}_2(t)$ (circles). (b) Prediction over the whole transient of the model calibrated on the time range 28.4–35.6: comparison between the mode amplitude from model integration $a_2(t)$ (thick line) and numerical simulation $\hat{a}_2(t)$ (circles).

Denote by $\boldsymbol{\Phi}$ the matrix whose columns are the POD modes retained in the model, arranged in vectors with the same rules as those by which the Navier–Stokes solution is arranged in $\boldsymbol{\psi}$. We have $\boldsymbol{\Phi}^{\mathrm{T}}\boldsymbol{\Phi} = \mathbf{I}$ for the orthonormality of the POD modes. Let $\boldsymbol{a}(t) = [a_1(t), \ldots, a_{N_m}(t)]^{\mathrm{T}}$ and $\tilde{\boldsymbol{\psi}}(t) = \boldsymbol{\Phi}\boldsymbol{a}(t)$, then Eq. (8) premultiplied by $\boldsymbol{\Phi}$ reads $\tilde{\boldsymbol{\psi}}_t \simeq \boldsymbol{\Phi}\mathbf{J}\boldsymbol{\Phi}^{\mathrm{T}}\tilde{\boldsymbol{\psi}}$;

by comparing this equation with (10) the estimate $\tilde{\mathbf{L}} = \boldsymbol{\Phi}\mathbf{J}\boldsymbol{\Phi}^{\mathrm{T}}$ for the linearized Navier–Stokes operator $\mathbf{L}$ is found. On the other hand, by construction, we have that $\mathbf{J} = \boldsymbol{\Phi}^{\mathrm{T}}\mathbf{L}\boldsymbol{\Phi}$.

The solution of the linearized low-order model equation (9) matches exactly the projection of the Navier–Stokes data over the POD modes (Fig. 3). Hence, it can be used to estimate the solution in the physical space by writing

$$\tilde{\boldsymbol{\psi}}(t) = \boldsymbol{\Phi}\boldsymbol{a} = \boldsymbol{\Phi}\mathbf{Q}\exp(\boldsymbol{\Lambda}t)\mathbf{Q}^{-1}\boldsymbol{\Phi}^{\mathrm{T}}\boldsymbol{\psi}_0. \tag{12}$$

We recall that λ_1 and λ_2 have positive real part and the corresponding unstable eigenvectors occupy the first two columns of $\mathbf{Q}$. Accordingly, we assume that the eigenvalues which correspond to the physical unstable mode are σ_1 and σ_2 ($\mathrm{Re}(\sigma_{1,2}) > 0$) with the physical unstable eigenvectors arranged in the first two columns of $\mathbf{P}$.

Let us denote with $\mathcal{P}$ and $\mathcal{P}^\star$ the submatrices formed by the first two columns of $\mathbf{P}$ and by the first two rows of $\mathbf{P}^{-1}$ respectively. Similarly, let us denote with $\mathcal{Q}$ and $\mathcal{Q}^\star$ the submatrices formed by the first two columns of $\mathbf{Q}$ and by the first two rows of $\mathbf{Q}^{-1}$, respectively.

Then, by equating the physical solution (11) to its reconstruction (12), after having neglected the decreasing exponentials, it follows that

$$\mathcal{P}\begin{bmatrix} \mathrm{e}^{\sigma_1 t} & 0 \\ 0 & \mathrm{e}^{\sigma_2 t} \end{bmatrix}\mathcal{P}^\star\boldsymbol{\psi}_0 = \boldsymbol{\Phi}\mathcal{Q}\begin{bmatrix} \mathrm{e}^{\lambda_1 t} & 0 \\ 0 & \mathrm{e}^{\lambda_2 t} \end{bmatrix}\mathcal{Q}^\star\boldsymbol{\Phi}^{\mathrm{T}}\boldsymbol{\psi}_0.$$

Since $\sigma_{1,2} \approx \lambda_{1,2}$ to an high degree of accuracy, we obtain $\mathcal{P} \approx \boldsymbol{\Phi}\mathcal{Q}$ and $\mathcal{P}^\star \approx \mathcal{Q}^\star\boldsymbol{\Phi}^{\mathrm{T}}$. In order to give a graphical representation of the reconstructed physical unstable eigenvector we have drawn in Fig. 5(b) the modulus of the first column of $\mathcal{P}$. It is interesting to make a comparison with the real unstable eigenvector obtained by solving the eigenproblem associated to the full linearized Navier–Stokes operator $\mathbf{L}$. The numerical value for the latter depicted in Fig. 5(a), have been kindly provided by Flavio Giannetti who has repeated for the current geometry the same kind of calculation performed in his work with Paolo Luchini for the case of the circular cylinder [23]. The agreement is satisfactory, confirming the validity of the POD-Galerkin approach in the study of the stability.

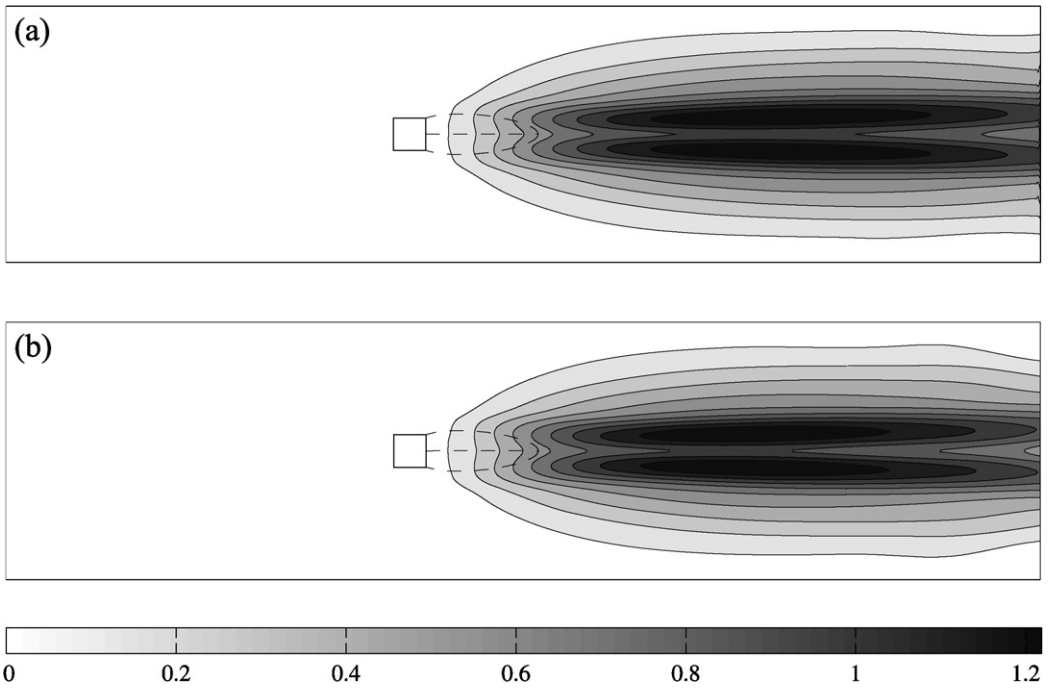

Fig. 5. (a) Spatial distribution of the modulus of the unstable eigenvector (data courtesy of Flavio Giannetti). (b) Spatial distribution of the modulus of the reconstructed unstable eigenvector.

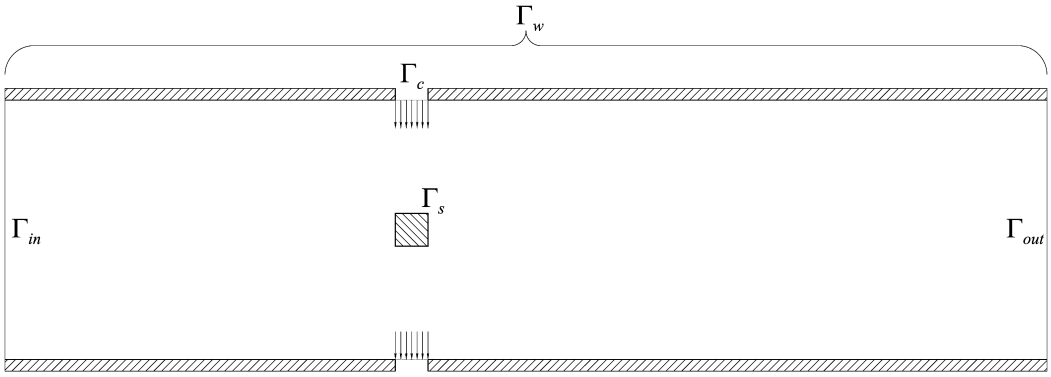

Fig. 6. Actuation scheme.

4. Low dimensional modeling of transversely forced flow

In this section we focus on the changes to be made in the POD-Galerkin model in order to obtain a proper simulation of the flow around the square cylinder when blowing/suction is performed along the channel walls. The velocity along the walls is everywhere zero except for two opposite segments next to the square where its transverse component varies in time, while remaining constant along the streamwise direction, that is $\boldsymbol{u}(\boldsymbol{x},t) = c(t)\,\boldsymbol{j}$ with $\boldsymbol{x} \in \Gamma_c$ (see Fig. 6). The actuators are driven in opposite phases, i.e. at any time the velocity vector of the top actuator is equal in amplitude to that of the bottom actuator, so that the flow rate through the channel does not change.

Let us define with $\bar{\boldsymbol{u}}'(\boldsymbol{x})$ our base state when $c(t) = c^\star = 0.1$, obtained just like in the unforced case when the numerical simulation reaches a minimum value in the time residual. It can be observed that the solution $\boldsymbol{u}_c(\boldsymbol{x}) = \bar{\boldsymbol{u}}'(\boldsymbol{x}) - \bar{\boldsymbol{u}}(\boldsymbol{x})$ is such that $\boldsymbol{u} = 0$ on $\Gamma_{\text{in}}, \Gamma_w - \Gamma_c$ and $\boldsymbol{u} = c^\star \boldsymbol{j}$ on Γ_c. The velocity field of the system which has been forced with a generic control law $c(t)$, is expressed as in [24] according to the following expansion

$$\boldsymbol{u}(\boldsymbol{x},t) = \bar{\boldsymbol{u}}(\boldsymbol{x}) + \frac{c(t)}{c^\star}\boldsymbol{u}_c(\boldsymbol{x}) + \sum_{n=1}^{N_m} a_n(t)\boldsymbol{\phi}_n(\boldsymbol{x}).$$

It turns out that the velocity is zero on $\Gamma_{\text{in}}, \Gamma_w$ for the filtered snapshots $\boldsymbol{u}(\boldsymbol{x},t_i) - \bar{\boldsymbol{u}}(\boldsymbol{x}) - c(t_i)\boldsymbol{u}_c(\boldsymbol{x})$, where for ease of notation we have renamed $c(t)/c^\star$ as $c(t)$. By substituting the former expansion into the Navier–Stokes equations and projecting onto the POD modes one obtains:

$$\begin{aligned}
&\dot{a}_r(t) = -(\nabla p, \boldsymbol{\phi}_r) + A''_r + C''_{kr}a_k(t) - B_{ksr}a_k(t)a_s(t) - E''_r\dot{c} - F''_r c^2 + \big(G''_r - H''_{kr}a_k\big)c,\\
&a_r(0) = \big(\boldsymbol{u}(\boldsymbol{x},0) - \bar{\boldsymbol{u}}(\boldsymbol{x}) - c(t)\boldsymbol{u}_c(\boldsymbol{x}), \boldsymbol{\phi}_r\big),
\end{aligned}$$

where all the subscripts run from 1 to N_m and

$$\begin{aligned}
&E''_r = (\boldsymbol{u}_c, \boldsymbol{\phi}_r),\\
&F''_r = (\boldsymbol{u}_c \cdot \nabla \boldsymbol{u}_c, \boldsymbol{\phi}_r),\\
&G''_r = (\Delta \boldsymbol{u}_c, \boldsymbol{\phi}_r)/Re - (\bar{\boldsymbol{u}} \cdot \nabla \boldsymbol{u}_c, \boldsymbol{\phi}_r), -(\boldsymbol{u}_c \cdot \nabla \bar{\boldsymbol{u}}, \boldsymbol{\phi}_r),\\
&H''_{kr} = (\boldsymbol{u}_c \cdot \nabla \boldsymbol{\phi}_k, \boldsymbol{\phi}_r) + (\boldsymbol{\phi}_k \cdot \nabla \boldsymbol{u}_c, \boldsymbol{\phi}_r).
\end{aligned}$$

We choose to model the projection term relevant to the pressure and the unresolved scales by assuming that

$$-(\nabla p, \boldsymbol{\phi}_r) = A'_r + C'_{kr}a_k(t) - E'_r\dot{c} - F'_r c^2 + \big(G'_r - H'_{kr}a_k\big)c,$$

where the primed quantities are unknown. By setting $A'_r = A_r - A''_r$, $C'_{kr} = C_{kr} - C''_{kr}$, $E'_r = E_r - E''_r$, $F'_r = F_r - F''_r$, $G'_r = G_r - G''_r$ and $H'_{kr} = H_{kr} - H''_{kr}$, the former system can be rewritten

$$\begin{aligned}
&\dot{a}_r(t) = A_r + C_{kr}a_k(t) - B_{ksr}a_k(t)a_s(t) - E_r\dot{c} - F_r c^2 + (G_r - H_{kr}a_k)c,\\
&a_r(0) = \big(\boldsymbol{u}(\boldsymbol{x},0) - \bar{\boldsymbol{u}}(\boldsymbol{x}) - c(t)\,\boldsymbol{u}_c(\boldsymbol{x}), \boldsymbol{\phi}_r\big).
\end{aligned}$$

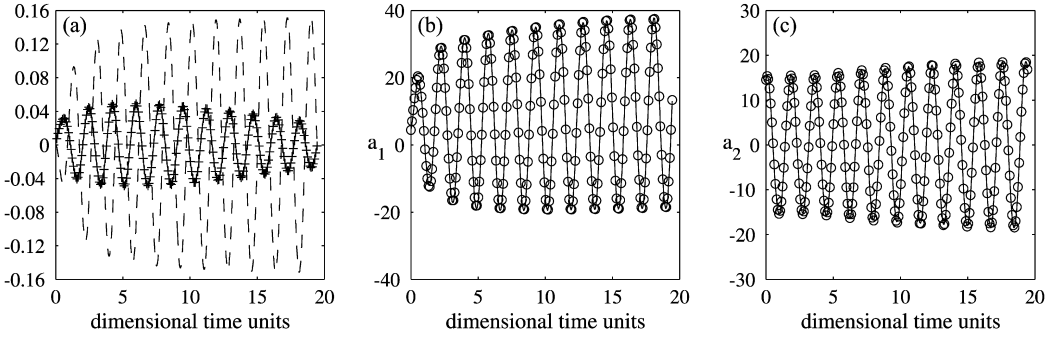

Fig. 7. (a) Lift versus time ("+") and forcing law (dashed line); (b) coefficient a_1 and (c) coefficient a_2: model integration (solid lines) and projection of the full numerical simulation (circles) versus time.

In other words the calibration procedure is performed for every projection term except for B_{ksr}.

We considered a numerical simulation at a Reynolds number of $Re = 60$, which is slightly greater than the critical value of 57. In this case the lift oscillates between -0.02 and 0.02 for the fully developed flow. Once the limit cycle has been reached, we set $t = 0$ for the instant corresponding to zero lift and apply the following forcing law $c(t) = -2/\pi \sin(2\pi t T_{\text{ref}}/T_S) \arctan(t T_{\text{ref}})$, where T_S denotes the dimensional period of the limit cycle oscillations. The forcing is chosen such that its amplitude reaches gradually the asymptotic value. In Fig. 7(a) both the lift and the forcing are shown as a function of the dimensional time.

A numerical database has been built by sampling the time span between 0 and 19.45 with 222 snapshots (see 'plus' markers in Fig. 7(a)) and a POD base of $N_m = 5$ modes has been extracted from it with a reconstruction error of about 1.3%. The unknown A_r, C_{kr}, E_r, F_r, G_r and H_{kr} are determined according to the same procedure followed above for the modeling of the transient. The resulting direct-adjoint problem is then

$$\begin{cases} \dot{a}_r(t) = A_r + C_{kr}a_k(t) - B_{ksr}a_k(t)a_s(t) - E_r\dot{c} - F_r c^2 + (G_r - H_{kr}a_k)c, \\ a_r(0) = (\boldsymbol{u}(\boldsymbol{x},0) - \bar{\boldsymbol{u}}(\boldsymbol{x}), \boldsymbol{\phi}_r), \end{cases} \quad \text{direct problem,}$$

$$\begin{cases} -\dot{b}_r(t) = \big[C_{rk} - H_{rk}c(t) - (B_{lrk} + B_{rlk})a_l(t)\big]b_k(t) - 2\big[a_r(t) - \hat{a}_r(t)\big], \\ b_r(T) = 0, \end{cases} \quad \text{adjoint problem,}$$

$$\begin{cases} \int_0^T b_r(t)\,\mathrm{d}t = 0, \\ \int_0^T a_k(t)b_r(t)\,\mathrm{d}t = 0, \\ \int_0^T b_k(t)\dot{c}(t)\,\mathrm{d}t = 0, \\ \int_0^T b_k(t)c^2(t)\,\mathrm{d}t = 0, \\ \int_0^T b_k(t)c(t)\,\mathrm{d}t = 0, \\ \int_0^T a_k(t)b_r(t)c(t)\,\mathrm{d}t = 0, \end{cases} \quad \text{optimality conditions,}$$

that can be solved by means of the pseudo–spectral techniques employed previously. Typical results are depicted in Fig. 7 (b) and (c), where the first two computed coefficient are compared successfully to the corresponding projections. For a completely different control law, the prediction of the forced flow provided by the low order model might be poor. However, this is not crucial for control purposes. As a matter of fact, if a control law is obtained from the model and employed in a Navier–Stokes simulation yielding results different from predictions, a new model can be built from these new data and a new control law can be recomputed. This loop converges as it was shown in [13] and [24]. What is crucial in this iterative procedure, is to get a model that exactly reproduces the application of the control for a given case.

5. Conclusions

In this paper a pseudo-spectral method to obtain accurate low order models of transient phenomena has been described. The idea is to augment the POD-Galerkin model by a linear term whose coefficients are computed in order

to fit a reference solution. The accuracy of the fitting is attained by a spectral representation of the low order model solution. This approach guarantees a virtually exact dynamical representation of the large scale structures. It has been shown how the method can be employed to obtain a reasonably reliable surrogate to a full eigenmode analysis of the Navier–Stokes equations, when looking for the most unstable mode of a developing instability. An extension of this approach has been devised so as to encompass the modeling of flows under external actuation, providing a cheap and reliable plant model for control purposes. One of the main issues left open for investigation is how to take advantage of the perturbation analysis to efficiently modify the POD modes for flow regimes that are only slightly different from those used to generate the POD modes themselves. By doing so one would obtain a dramatic speed up in convergence to the optimal control when using for example the adaptive iterative procedure proposed in [24].

Acknowledgements

We are grateful to Flavio Giannetti for providing the data reported in Fig. 5(a).

References

[1] J.L. Lumley, The structure of inhomogeneous turbulent flows, in: A.M. Yaglom, V.L. Tatarski (Eds.) Atmospheric Turbulence and Radio Wave Propagation, Moscow, 1967, pp. 166–178.
[2] H. Telib, M. Manhart, A. Iollo, Analysis and low-order modeling of the inhomogeneous transitional flow inside a T-mixer, Phys. Fluids 8 (2004) 2717–2731.
[3] A.E. Deane, I.G. Kevrekidis, G.E. Karniadakis, S.A. Orszag, Low-dimensional models for complex geometry flows: Application to grooved channels and circular cylinders, Phys. Fluids A 3 (1991) 2337–2354.
[4] X. Ma, G.E. Karniadakis, A low-dimensional model for simulating three-dimensional cylinder flow, J. Fluid Mech. 458 (2002) 181–190.
[5] B.R. Noack, K. Afanasiev, M. Morzyński, G. Tadmor, F. Thiele, A hierarchy of low-dimensional models for the transient cylinder wake, J. Fluid Mech. 497 (2003) 335–363.
[6] N. Aubry, P. Holmes, J.L. Lumley, E. Stone, The dynamics of coherent structures in the wall region of a turbulent boundary layer, J. Fluid Mech. 192 (1998) 115–173.
[7] W. Cazemier, R.W.C.P. Verstappen, A.E.P. Veldman, Proper orthogonal decomposition and low-dimensional models for driven cavity flows, Phys. Fluids 10 (1988) 1685–1699.
[8] A. Iollo, A. Dervieux, J.A. Désidéri, S. Lanteri, Two stable POD-based approximations to the Navier–Stokes equations, Comput. Vis. Sci. 3 (1–2) (2000) 61–66.
[9] A. Iollo, S. Lanteri, J.A. Désidéri, Stability properties of POD-Galerkin approximations for the compressible Navier–Stokes equations, Theor. Comp. Fluid Dyn. 13 (6) (2000) 377–396.
[10] C.W. Rowley, T. Colonius, R.M. Murray, Model reduction for compressible flows using POD and Galerkin projection, Physica D 189 (2004) 115–129.
[11] S. Sirisup, G.E. Karniadakis, A spectral viscosity method for correcting the long-term behavior of POD models, J. Comput. Phys. 194 (2004) 92–116.
[12] B. Galletti, C.H. Bruneau, L. Zannetti, A. Iollo, Low-order modelling of laminar flow regimes past a confined square cylinder, J. Fluid Mech. 503 (2004) 161–170.
[13] M. Bergmann, L. Cordier, J.-P. Brancher, Optimal rotary control of the cylinder wake using POD reduced order model, Phys. Fluids 17 (2005) 097101.
[14] M. Couplet, C. Basdevant, P. Sagaut, Calibrated reduced-order POD-Galerkin system for fluid flow modelling, J. Comput. Phys. 207 (2005) 192–220.
[15] B.R. Noack, P. Papas, P.A. Monkewitz, The need for a pressure-term representation in empirical Galerkin models of incompressible shear flows, J. Fluid Mech. 523 (2005) 339–365.
[16] M. Breuer, J. Bernsdorf, T. Zeiser, F. Durst, Accurate computations of the laminar flow past a square cylinder based on two different methods: lattice-Boltzmann and finite-volume, Int. J. Heat Fluid Flow 21 (2000) 186–196.
[17] R.W. Davis, E.F. Moore, L. P Purtell, Numerical-experimental study of confined flow around rectangular cylinders, Phys. Fluids 27 (1984) 46–59.
[18] A. Okajima, Strouhal numbers of rectangular cylinders, J. Fluid Mech. 123 (1982) 379–398.
[19] H. Suzuki, Y. Inoue, Unsteady flow in a channel obstructed by a square rod (criss-cross motion of vortex), Int. J. Heat Fluid Flow 14 (1993) 2–9.
[20] L. Sirovich, Turbulence and the dynamics of coherent structures. Parts I, II and III, Quart. Appl. Math. XLV (1987) 561–590.
[21] C. Canuto, Y. Hussaini, A. Quarteroni, T. Zang, Spectral Methods in Fluid Dynamics, Springer, 1988.
[22] G. Tadmor, B.R. Noack, M. Morzyński, S. Siegel, Low-dimensional models for feedback flow control. Part II: Controller design and dynamic estimation, in: 2nd AIAA Flow Control Conference, Portland, Oregon, USA, June 28 – July 1, 2004, AIAA Paper 2004-2409, 2004, pp. 1–12.
[23] F. Giannetti, P. Luchini, Receptivity of the circular cylinder's first instability, in: Euromech Fluid Mechanics Conference, Toulouse, France, 2003.
[24] S.S. Ravindran, Control of flow separation over a forward-facing step by model reduction, Comput. Methods Appl. Mech. Engrg. 191 (2002) 4599–4617.